Instruments and Methods

Estimates of the refreezing rate in an ice-shelf borehole

Kenneth G. HUGHES,[1] Pat J. LANGHORNE,[1] Michael J.M. WILLIAMS[2]

[1] *Department of Physics, University of Otago, Dunedin, New Zealand*
E-mail: kenneth.hughes@otago.ac.nz
[2] *National Institute of Water and Atmospheric Research Ltd (NIWA), Wellington, New Zealand*

ABSTRACT. The refreezing rate of a borehole drilled through a 252 m thick region of the Ross Ice Shelf, Antarctica, is determined using oceanographic measurements over two periods of a day. We first use a method based on the conservation of salt in the supercooled salt water of the borehole. This is compared to a model using a numerical solution of the heat equation to find the temperature distribution in the host ice, allowing ice growth to be calculated from the balance of heat fluxes at the ice/water interface. This second method broadly confirms the refreezing rates deduced from salinity measurements, giving confidence in the generalization of this simple heat-flux model to predict refreezing rates of other boreholes. Predictions from both are subject to uncertainty due to the poorly defined value of the solid fraction of ice that freezes in a supercooled volume of sea water. This is taken to be 0.5 ± 0.1 throughout this study. The predicted rates are also strongly dependent on the initial and boundary conditions chosen, but results show the initial diameter of 600 mm decreases at a rate of $\sim$3–5 mm h^{-1} in an ice shelf with a minimum temperature of –22°C.

INTRODUCTION

Hot-water drilling of a borehole through an ice shelf allows access to the cavity below for oceanographic and geological research (e.g. Jacobs and others, 1979; Foster, 1983). These long, cylindrical, saltwater-filled holes begin refreezing immediately after their creation. For safe retrieval of instruments, the hole cannot be left to refreeze until its diameter becomes less than the size of the instruments being lowered through the hole. However, the closure is not easily logged and the creation of a model of ice growth in the borehole allows for the a priori prediction of the length of time the hole can be used.

This study aims to model the refreezing of a $\sim$600 mm diameter borehole drilled through the Ross Ice Shelf (Fig. 1) as part of an ANtarctic geological DRILLing (ANDRILL) project undertaken in November and December 2010. The borehole, located at 77°31.558′ S, 171°20.138′ E, was in a region where the ice shelf was 252 m thick and had an ocean depth of 901 m. It was one of four holes drilled using an ANDRILL-operated hot-water drill as part of their site survey at Coulman High, with the primary aim of understanding the marine environment under the ice shelf (Rack and others, 2012).

The mechanism and rate at which ice forms in a borehole is affected by the temperature of the surrounding 'host' ice, the depth of the hole and whether fresh water or sea water occupies the hole. Harrison (1972) equates the energy used by a thermal drill to that required to melt a particular volume of refrozen ice inside the borehole, and finds a refreezing rate of the order of a millimetre per week in temperate ice. This is far slower than for cold ice, as studied here, where refreezing occurs at a rate of the order of millimetres per hour in ice at −20°C. Humphrey and Echelmeyer (1990) apply a one-dimensional finite-element model to calculate the evolution of the radii of boreholes in Whillans Ice Stream, Antarctica and Jakobshavn Isbræ, Greenland, with depths of 1050 and 1630 m, respectively. The two markedly different vertical temperature profiles associated with these glaciers allow the results to be adapted to a wide range of locations. The structure of ice that grows inside these holes filled with fresh water is assumed to be no different from that of the solid host ice. However, in supercooled salt water, as in our study, ice often forms with an open, porous structure. Several other mathematically rigorous studies have considered the problem of a freezing interface moving in a radial direction (e.g. Kreith and Romie, 1955; Poots, 1962), but their application to this study is limited as they do not consider the possibility of the solid being porous.

Refreezing rates have been measured directly in a borehole drilled through a 562 m thick region of the Ronne Ice Shelf, Antarctica (Makinson, 1993). Despite the difference in ice-shelf thicknesses, his results are comparable to our study because the undisturbed temperature through the ice shelf varies with depth in a similar way. Successive calliper profiles taken shortly after the Ronne Ice Shelf hole was drilled indicated initial closure rates of 9–11 mm diameter h^{-1} for a 0.13 m diameter hole in ice at −26°C. After the hole had been kept open for 2 days, and the host ice had warmed, this rate had dropped to 4–5 mm h^{-1}.

An important consideration in this study is the nature of the refreezing interface. From direct observation we know that the borehole contains supercooled water, i.e. water below its freezing point (Fig. 2d and h). Once refreezing begins, down-hole video recordings (Fig. 3) show evidence of small ice crystals accreted to the walls of the hole in areas known to be supercooled. The crystals were not firmly attached and were dislodged when the wall was scraped by instruments. These crystals were then suspended in the water column. No direct measurements of crystal size were made. However, inspection of the video shows similar sizes of crystals to those reported by Gough and others (2012), of the order of millimetres. We anticipate there are also smaller-diameter crystals, but are unable to accurately estimate a lower bound on crystal size. Attachment and

https://doi.org/10.3189/2013JoG12J117 Published online by Cambridge University Press

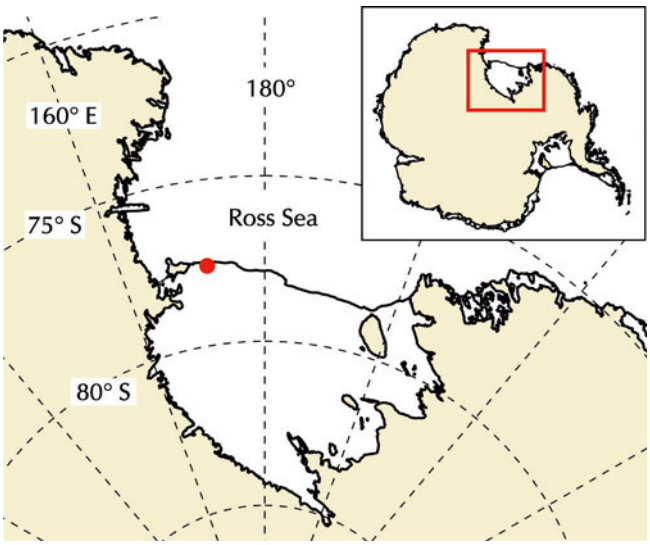

Fig. 1. Map showing the location of the borehole on the Ross Ice Shelf (red dot), where the ice was 252 m thick.

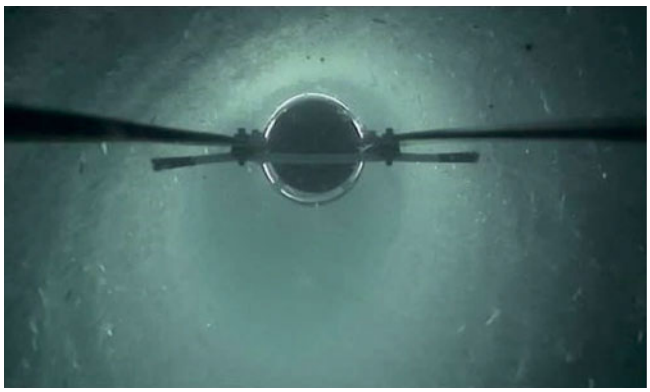

Fig. 3. A still image from the down-hole video recording. The camera is looking down onto the bag of the light housing. Ice crystals can be seen loosely accreted to the hole walls. Detached ice crystals can also be seen in suspension floating across the back of the light housing.

growth of crystals on the borehole wall led to a porous annulus of ice down the entire depth of the hole. This is similar to the growth of ice on vertical ropes in supercooled water next to ice shelves (Leonard and others, 2006; Mahoney and others, 2011). Beneath sea ice, accumulation and growth of suspended crystals results in the sub-ice platelet layer, which is known to be porous and permeable (Gough and others, 2012).

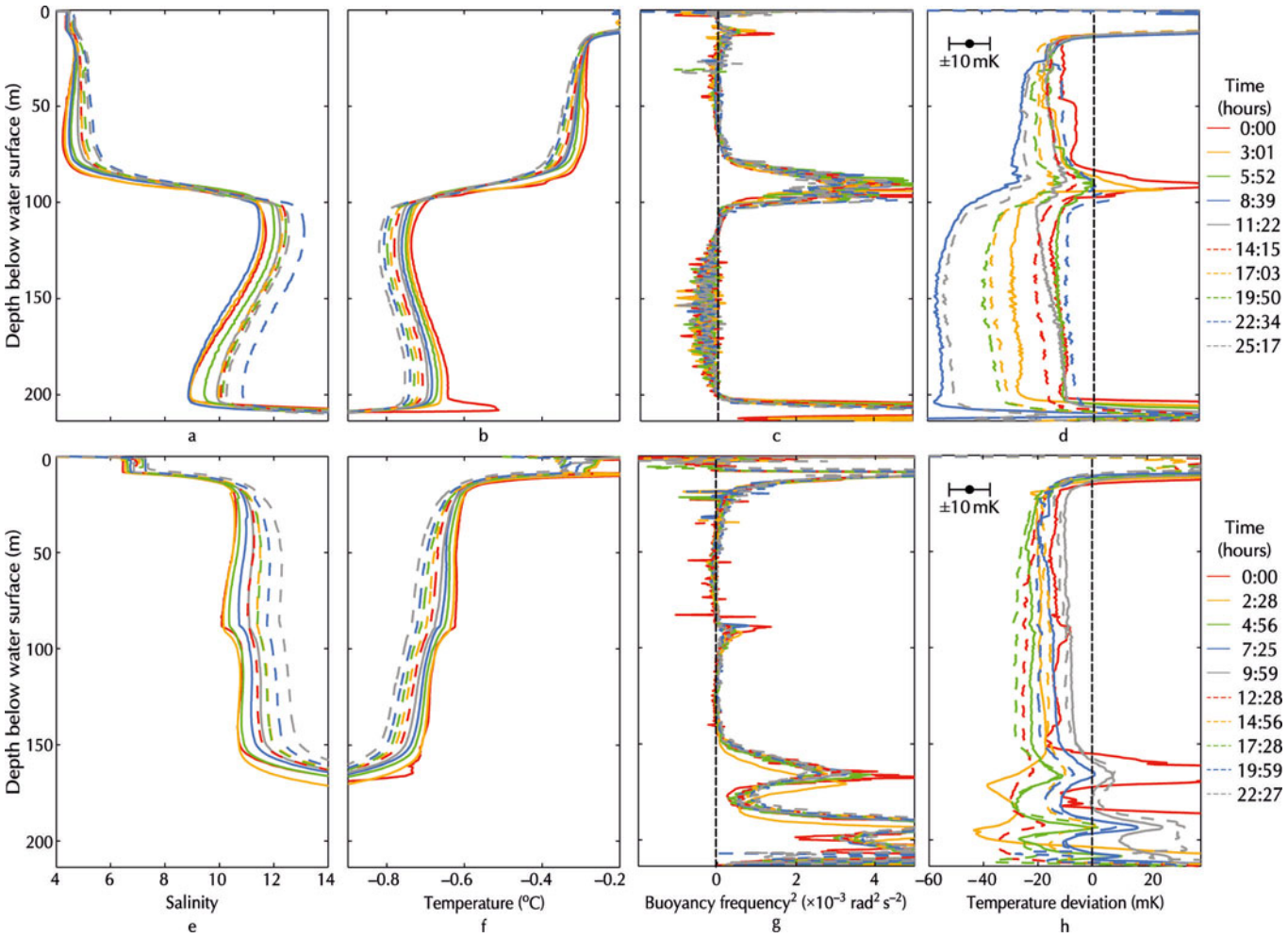

Fig. 2. The variation, with water depth and time, of salinity, temperature, buoyancy frequency squared and deviation of temperature from freezing point (negative values indicate supercooling). (a–d) The ten oceanographic casts starting at 03:12 8 December 2010 (UT); (e–h) casts starting at 23:09 12 December 2010 (UT). Plots are truncated to enlarge the region of interest. The legends refer to the number of hours and minutes at which each cast started relative to the first. The uncertainty in the supercooling measurement is shown in the appropriate panels.

https://doi.org/10.3189/2013JoG12J117 Published online by Cambridge University Press

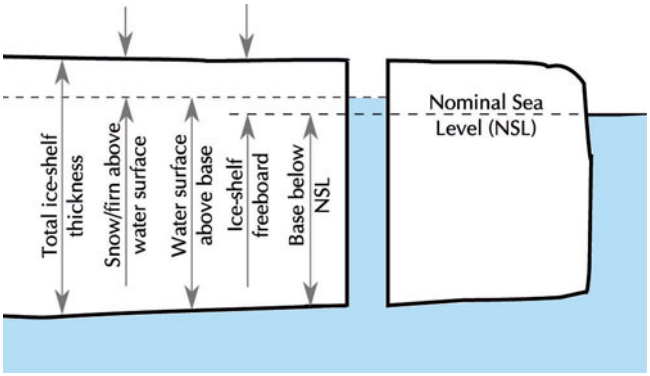

Fig. 4. Cross-sectional view of an ice shelf, showing the heights of significance (values given in Table 1).

We therefore define a parameter, ϕ, as the fraction of solid ice in a particular volume of supercooled water and assume its value is low enough that the liquid fraction is interconnected. This assumption was used in a successful model of refreezing sea-ice cracks (Petrich and others, 2007) of similar width scale to the diameter of the hole in our study. We use the sub-ice platelet layer as an analogue for ice that forms in a borehole, to provide a first estimate of the solid fraction. Like the sub-ice platelet layer, ice formation at the borehole wall has two main contributions: (1) ice forms due to heat transfer through the ice/water interface and (2) ice forms when ice crystals suspended in supercooled water attach to the interface.

We describe this process in this paper and provide a prediction of the refreezing of an ice-shelf borehole.

METHOD

The borehole was created in three stages. First, a well was formed to a depth of ~50 m below the ice-shelf surface. This was later used to hold water that was pumped to the surface to be warmed. Second, a thin pilot hole was melted through the ice shelf to establish a hydraulic connection to the ocean. Third, the hole was reamed to enlarge the diameter. A second reaming was completed 5 days after the first to widen the hole for further use. This process cannot be expected to produce a perfectly uniform borehole, yet down-hole video recordings showed that the hole was approximately cylindrical. The refreezing rates predicted in this study will treat the borehole as a cylinder of constant initial radius. As time progresses, the radius becomes a function of depth. Two approaches will be taken to calculate the change in radius with time. The first applies the principle of salt mass conservation to down-hole, oceanographic measurements. The second considers a heat budget and may be generalized to different boreholes.

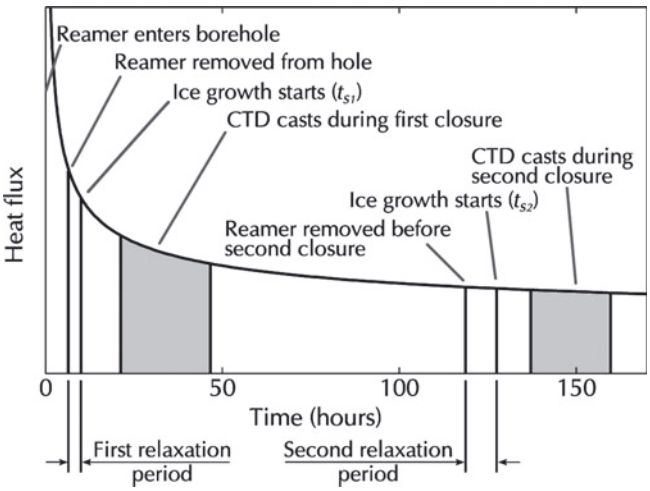

Fig. 5. Timeline of important events described in the text and the modelled heat flux (Eqns (3–6)) through the borehole wall. The reamer first entered the borehole at 04:58 7 December 2010 (UT).

Table 1. Significant measurements at the borehole site, not all of which are independent. NSL denotes nominal sea level

	Height m	Error m
Total ice-shelf thickness	252	1
Water surface above base	213.6	1
Snow/firn above water surface	38.5	1
Ice-shelf base below NSL	209	1
Water level in hole above NSL	4.6	0.1
Ice-shelf freeboard	43.1	1

Figure 4 shows all heights of significance; their respective values are given in Table 1. The water surface above the ice-shelf base was found by integrating the density of water within the hole from the surface to the known pressure at the base. This known pressure can be converted to a depth below nominal sea level (NSL) by assuming sea water has a fixed temperature and salinity of 0°C and 35, respectively (Fofonoff and Millard, 1983), and is equivalent to the sea level in front of the ice shelf. The water level above NSL is independent of the basal pressure and can be calculated accurately. Depths will be described relative to the surface of the water in the hole hereafter.

The data used in this study were collected over two 28 hour periods. During each period a Sea-Bird Electronics SBE19+ conductivity–temperature–depth (CTD) profiler was deployed ten times from the ice-shelf surface to measure temperature and salinity in the sub-ice-shelf ocean (Fig. 2). In each of the ten casts the profiler descended and ascended through the borehole once; only downcasts will be used here. The manufacturer's stated accuracies for temperature and salinity are 5 mK and 0.004, respectively and resolutions are 0.1 mK and 0.0004, respectively.

The first and second 28 hour periods began respectively at 03:12 8 December 2010 (UT) and 23:09 12 December 2010 (Fig. 5). These times correspond to 15 and 18 hours after the hole was first reamed and re-reamed, respectively. We introduce the terms 'first closure' and 'second closure' to describe the periods after successive reamings. The profiler in its frame used in this study had a maximum diameter of 225 mm. This value provides a minimum diameter for the borehole and will be used as a first check of the results. Video was used to judge the diameter of the hole. Using a 400 mm bar in front of the camera for scale, the recently reamed hole diameter was judged to be 600 ± 50 mm.

Figure 6 shows the down-hole temperature and salinity averaged over the ten casts during the first and second closures. The water in the borehole is ~1°C warmer, three to nine times less saline and displays stronger gradients than the

https://doi.org/10.3189/2013JoG12J117 Published online by Cambridge University Press

ocean below. The large gradients in both temperature and salinity evident at ~85 m depth are attributed to the hose stopping for a period of ~5 min at this depth to allow a hose coupling to pass through the drilling system. The lower salinity and higher temperature above 85 m are explained by the consequent addition of heat and meltwater. In other parts of the hole the salinity profile is nearly vertical as a result of the intense vertical mixing produced during reaming.

The temperature and salinity for individual casts, as well as the derived properties of buoyancy frequency and supercooling, are shown for all casts in Figure 2. The buoyancy frequency is the frequency at which a displaced water parcel will oscillate within a stable water column. The square of its value, which is proportional to the vertical density gradient, is positive if the water column is stable. Negative values indicate unstable stratification. The values at the base of the hole are particularly large, due to a strong density gradient. This indicates that the water in the hole is effectively isolated from the ocean below.

Buoyancy-driven convection, from salt rejection during freezing, will be governed by the confines of the hole. Experiments involving an unstable gradient inside a tall, vertical cylinder by Cholemari and Arakeri (2009) showed that the system's potential energy is converted to turbulent kinetic energy over length scales up to and approximately equal to the diameter of the hole. Using flow visualization techniques, they demonstrated that flow became decorrelated over length scales greater than the diameter. Undertaking a similar experiment, Arakeri and others (2000) found that when the flow became turbulent, which we expect in the present case based on the Rayleigh number in the hole (Appendix A), there were no two clear streams of upward- and downward-flowing fluid. Their scaling arguments suggest that the unstable gradients that we observe within the borehole would decay approximately exponentially over a characteristic timescale of 2–10 hours, depending on the hole's diameter and the height of the instability. At 100–200 m during first closure, we observed unstable stratification to persist over the entire measurement period (Fig. 2c), i.e. longer than 2–10 hours, and attribute its longevity to the continual rejection of salt into the water column, which likely occurs more slowly closer to the base as the surrounding ice temperature decreases.

The buoyancy-driven turbulence described above is augmented by movement of the CTD profiler through the hole and the growth of ice at the walls. The former process provides mechanical mixing; the latter influences local velocities through the introduction of salt and heat gradients at the growing interface (Huang and Barduhn, 1985).

CLOSURE DERIVED FROM SALINITY MEASUREMENTS

We treat the borehole as a closed system because of the stable gradients at the bottom of the hole. Thus the salinity of water in the borehole increases as the hole closes, because the mass of salt in the hole stays approximately constant while the volume of water containing the salt decreases. The refreezing rate calculation requires a number of assumptions, the most important of which are discussed below.

The solid fraction of ice, ϕ, is 0.5 ± 0.1. Gough and others (2012) determine the solid fraction in a sub-ice platelet layer using measurements of heat flux derived from sea-ice temperature profiles. They calculate a value of $\phi = 0.25 \pm 0.06$ in recently forming sea ice. In addition, they collate other published values, found using a variety of methods, with a range of 0.2–0.5. Some care must be taken in treating the refrozen ice in a borehole as a sub-ice platelet layer. On average, buoyant frazil crystals rise vertically upward, i.e. perpendicular to a horizontal surface. Consequently, fewer crystals will be deposited onto an approximately vertical wall than onto a horizontal one. We therefore expect congelation and interstitial growth would have a greater effect on ice formation in the borehole, leading to a higher solid fraction than that for the sub-ice platelet layer. For this reason and from visual inspection of ice formation on ropes hanging vertically in the upper ocean (e.g. Mahoney and others, 2011) we use the largest of the values given by Gough and others (2012) as our estimate.

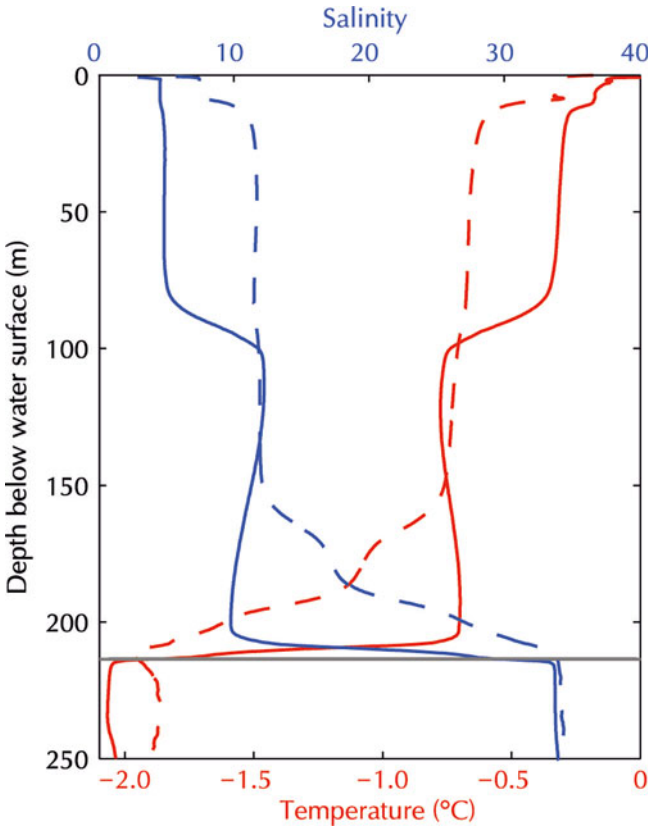

Fig. 6. Mean temperature and salinity of casts starting 03:12 8 December 2010 (solid curve) and 23:09 12 December 2010 (dashed curve). Times given in UT. The horizontal grey line indicates the base of the borehole.

In regions of unstable stratification, turbulent diffusion will redistribute salt over tens of metres between successive CTD casts. This redistribution will act to smooth out any depth dependence in the results, and hence entail additional uncertainty. Lacking detailed knowledge of the rate of redistribution, we reduce its uncertainty in the first instance by depth-averaging results into either 20 or 40 m depth bins.

The volume change as water turns to ice is ignored. The specific volume of ice is ~10% larger than that of the water inside the hole. The additional space required by the ice is produced by displacing water downward to maintain hydrostatic equilibrium. Based on the predicted

https://doi.org/10.3189/2013JoG12J117 Published online by Cambridge University Press

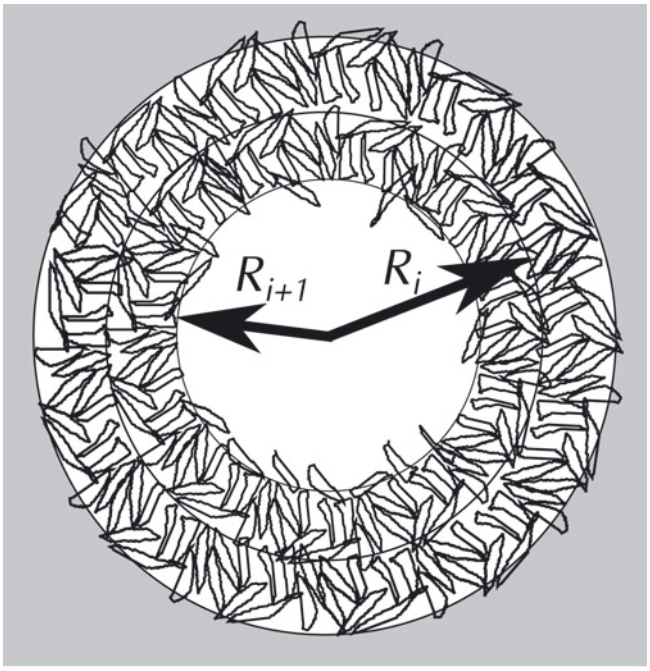

Fig. 7. Cross-sectional view of the growth inside the borehole. The radius at time t_i is the average position of the diffuse interface. The shaded background represents the solid ice through which the hole was drilled, whereas the refrozen annulus is a mix of ice and sea water. Not to scale.

ice growth rates we estimate that this results in a maximum advection of 4 m of water, i.e. 2% of the water height, through the bottom of the hole over 24 hours.

Considering Figure 7, the radius, R, is calculated each time the CTD profiler descends and these times are denoted t_i. After a period of growth, $t_{i+1} - t_i$, R_i becomes R_{i+1} and the salt, which was assumed to be uniformly distributed throughout the hole, can be found in any one of three regions: (1) in the salt water contained in the now smaller hole; (2) in the liquid fraction of the refrozen annulus; or (3) in the solid ice fraction of the refrozen annulus. It is well known that the salinity of solid ice is very close to zero since almost all salt is rejected into the sea water upon freezing (Weeks, 2010). Hence, we assume a salinity of zero for the ice.

Table 2. Variables used in salinity-derived closure calculations

Symbol	Description
a	Initial radius of the hole after reaming
A_i'	Volume per unit height of refrozen annulus
R_i	Radius of hole at time t_i
R_0	Radius of hole when CTD casts began
S_i	Salinity of water at time t_i
t_i	Times the hole radius is calculated (which are dictated by the times CTD profiles were taken)
V_i'	Volume per unit height of cylinder of radius R_i
ρ_i	Density of water at time t_i
ϕ	Fraction of solid ice in refrozen annulus

Applying conservation of mass of salt imposes (see Table 2 for variables):

$$\rho_i S_i V_i' + \rho_i S_i A_i'(1-\phi) = \rho_{i+1} S_{i+1} V_{i+1}' + \rho_{i+1} S_{i+1} A_{i+1}'(1-\phi) \quad (1)$$

where salinity is taken to be grams of salt per kilogram of salt water.

The left- and right-hand sides of Eqn (1) indicate the distribution of salt at times t_i and t_{i+1}, respectively. The first terms give the mass of salt per unit height inside the water-only region of the hole. The second terms give the mass of salt in the liquid fraction of the refrozen annulus, i.e. the region between R and a.

We rewrite V_i' and A_i' in terms of R_i, R_{i+1} and a, ignore the difference of <0.1% between ρ_i and ρ_{i+1}, and solve for R_{i+1} in terms of R_i and the salinity values to obtain

$$R_{i+1} = \sqrt{\frac{a^2(S_i - S_{i+1})(1-\phi) + R_i^2 S_i \phi}{S_{i+1}\phi}} \quad (2)$$

Because R_{i+1} is found recursively in terms of R_i each salinity measurement will affect the value calculated for the radius at all successive values of t_i. The procedure used to reduce any error associated with this effect is outlined in Appendix B.

The refreezing rates determined using the method outlined above, with $\phi = 0.5$, are shown in Figure 8, averaged over 40 m depth bins. The results are normalized with

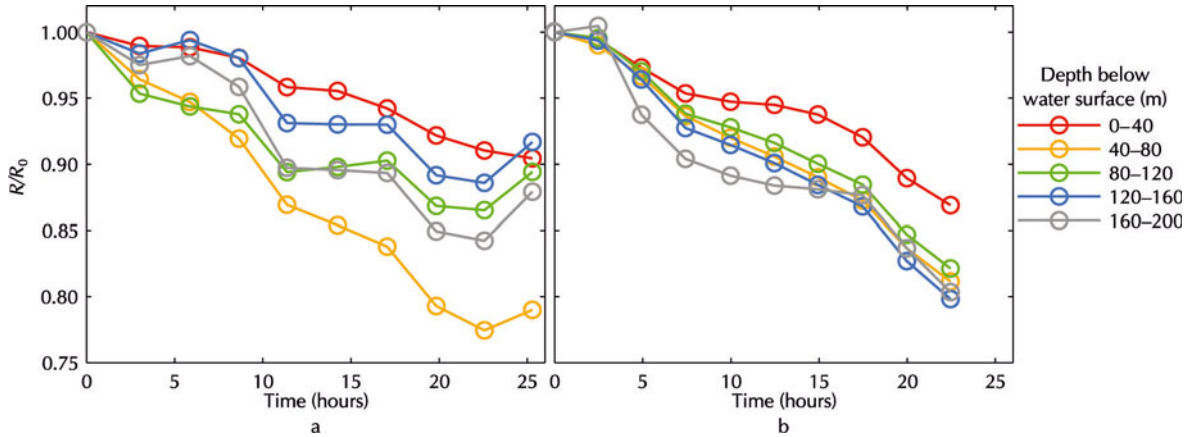

Fig. 8. The change in radius calculated from salinity measurements starting (a) 03:12 8 December 2010 (UT) and (b) 23:09 12 December 2010 (UT). The radii, averaged in 40 m depth bins, are non-dimensionalized and time is measured relative to the first cast in each set. R_0 is estimated to be 0.28 m and $\phi = 0.5$.

https://doi.org/10.3189/2013JoG12J117 Published online by Cambridge University Press

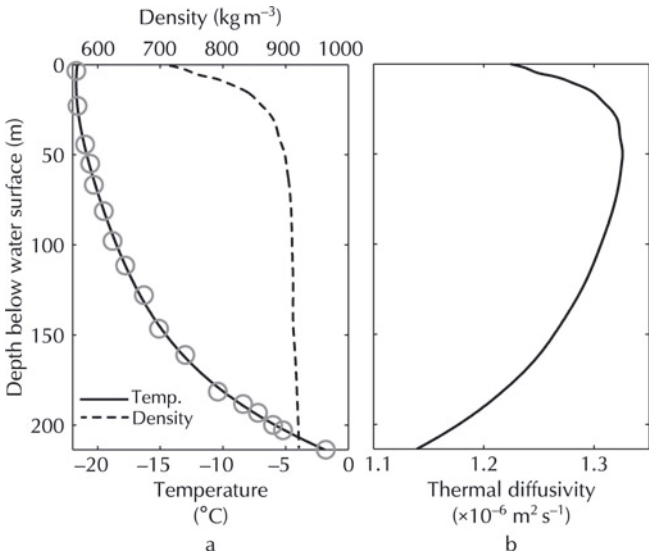

Fig. 9. (a) Temperature and density profiles through the ice shelf (Bender and Gow, 1961). Both the vertically scaled raw temperature data (circles) and fit used in this study (solid curve) are shown. (b) The variation of thermal diffusivity of ice with depth.

Table 3. Variables used in the heat-flux model

Parameter	Symbol	Unit	Value/range
Initial radius	a	m	0.3
Area of annulus	A'	m^2	
Specific heat capacity (ice)	c	J kg^{-1} K^{-1}	(1.94–2.09)×10^3
Heat flux	f	W m^{-2}	
Thermal conductivity (ice)	K	W m^{-1} K^{-1}	1.70–2.33
Latent heat of freezing	L_f	J kg^{-1}	3.35 × 10^5
Radial position	r	m	
Position of the ice/water interface	R	m	
Sum of reaming period and relaxation time	t_{s1} or t_{s2}	s	420–620 min or 123 hours
Host ice temperature	T	°C	
Undisturbed ice temperature	T_{ice}	°C	−21.7 to −1.9
Temperature (water)	T_w	°C	−2 to 0
Depth below water surface	z	m	
Thermal diffusivity (ice)	κ	m^2 s^{-1}	(1.14–1.33)×10^{-6}
Density (ice)	ρ	kg m^{-3}	718–917
Solid fraction	ϕ	dimensionless	0.5 ± 0.1

respect to R_0, the hole's radius at the time the calculation begins. R_0 differs from a due to the growth of ice during the 15 or 18 hour period after reaming ceased, but before CTD casts began. By extrapolation of the salinity-deduced closure rates, we estimate R_0 as 0.28 m. The region below 200 m is not considered, as the assumption of a closed system breaks down when very near the ocean.

HEAT-FLUX MODEL

A model of the refreezing rate in the borehole is developed using the balance between the source of latent heat of freezing and the divergence of conductive heat flux at the freezing interface. The model involves three steps. First, the temperature field in the host ice is determined as a function of depth, radial position and time. The need for a third spatial dimension is precluded as cylindrical symmetry is assumed. Second, the heat flux at the interface is determined. Third, the rate of ice growth is calculated by equating this heat flux to a phase change.

The depth-dependent thermal parameters included in this model are given in Table 3. The most important is the ice temperature. However, there are very few temperature profiles through ice shelves available. We use the data of Bender and Gow (1961) as they were taken in the Ross Ice Shelf, were measured at a similar distance from the ice-shelf edge and little change in temperature is expected since their measurements. The ice temperature in our model (Fig. 9a) uses a polynomial fit to these temperature measurements. A vertical scaling of 3% was required to adapt for the slight difference in ice-shelf thickness between our scenario and that of Bender and Gow (1961). The density profile (Fig. 9a) was also taken from Bender and Gow (1961). This was then used to calculate thermal conductivity, by assuming density variation was due to spherical air bubbles trapped in the ice (Schwerdtfeger, 1963). Temperature-dependent, tabulated values were used for specific heat capacity (Haynes, 2010). From these last three parameters the thermal diffusivity was calculated (Fig. 9b). Relatively smaller values of thermal diffusivity near the ice surface are caused by the lower density of the ice, whereas at the bottom the higher temperatures cause lower thermal diffusivities.

Because the values of many of these parameters vary with temperature they would naturally change as the ice surrounding the borehole warms. In this study they are taken to vary with depth, but this warming effect is not considered. The thermal diffusivity is only 16% lower for the warmest ice present in this study in comparison with the coldest. Other parameters vary with temperature by <10%.

The borehole is modelled as a cylinder composed of a large number of stacked discs. All parameters that vary with depth are discretized and any vertical heat transfer is negligible, because the vertical temperature gradients in the water and host ice are typically two orders of magnitude smaller than those in the radial direction. Hence, we require the temperature of the host ice in the region $r \geq a$ as a function of only radial position and time, from which we derive the heat flux and consequent ice growth. Any heat flux from the ocean is considered negligible, due to our contention that the hole is effectively isolated from the ocean beneath.

The ice shelf is assumed to be isotropic and contain no heat sources. Heat conduction is therefore governed by (see Table 3 for definition of variables):

$$\frac{\partial^2 T}{\partial r^2} + \frac{1}{r}\frac{\partial T}{\partial r} = \frac{1}{\kappa}\frac{\partial T}{\partial t} \tag{3}$$

Boundary conditions are required at the borehole surface and at points very far from the borehole:

$$T(r = a) = Tw \tag{4}$$

$$T(r \to \infty) = T_{ice} \tag{5}$$

Carslaw and Jaeger (1959) present the analytical solution to this partial differential equation, but their solution is given in terms of an integral containing a singularity at the lower limit of integration. Here we find the solution numerically using the MATLAB function 'pdepe'. Logarithmically spaced grids for r and t were used to give increased resolution for small values. Once the temperature is known as a function of radial position and time by solving Eqn (3), the flux through

https://doi.org/10.3189/2013JoG12J117 Published online by Cambridge University Press

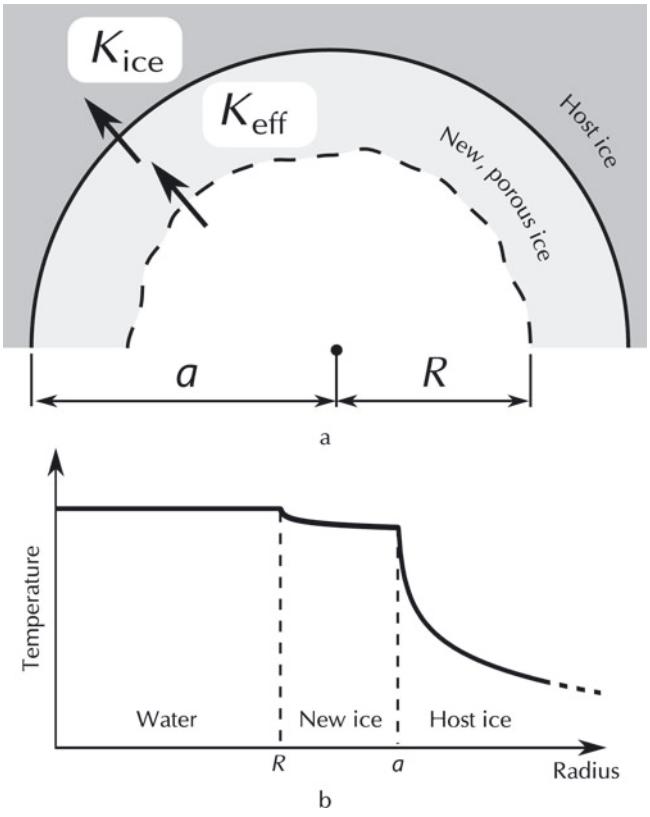

Fig. 10. (a) Cross-sectional view of half of the borehole, showing the different regions of ice and water and their respective thermal conductivities. An arrow represents a heat flux across the surface. (b) Expected temperature distribution in the water, new ice and host ice.

the borehole wall at any depth, z, can be found. For conduction through the cylindrical surface, $r = a$, the heat flux is given by

$$f_{ice} = -K\left[\frac{\partial T}{\partial r}\right]_{r=a} \tag{6}$$

This formulation does not account for two effects: the thermal energy added to the host ice during drilling and the movement of the ice/water interface. Each of these will be explained in turn. Creation of the pilot hole will add some thermal energy to the host ice, but the smaller diameter of the pilot hole means most of this warmed ice is later reamed. Thus drilling of the pilot hole will be ignored. The thermal energy added during reaming is accounted for by allowing the temperature field to evolve in the host ice for a specified period of time, with no ice growth taking place. This period ends when the water in the borehole has cooled to its freezing point. This warming of the host ice due to the loss of sensible heat from the water is shown schematically in Figure 5 as the initial rapid decrease in the heat flux through the hole wall, ending when ice growth begins at the end of the 'first relaxation period'.

Immediately after the second reaming (see Fig. 5) there is a time period, 'second relaxation period', during which the water in the hole loses sensible heat that was added during reaming. A single water temperature profile was measured 1 hour after reaming and showed the water was ~4°C above its freezing point. The time required to remove this sensible heat was estimated from the rate of total heat loss to the host ice, i.e. integrating the heat flux (Eqn (6)) over the total area of the borehole wall. The rate of total heat loss after the first reaming is approximately three times larger than that for the second reaming. Thus the first relaxation period is ~3 hours. It is assumed melting does not occur during the relaxation period, and ice growth commences once this period ends.

At any depth, the warming of the host ice, and the calculation of heat flux through the surface, begins the moment the reamer first reaches that depth. The first reaming took 440 min and the ice-shelf base was reached after 200 min. Depending on depth, the hole was therefore open for 240–440 min before the reamer was removed. We assume a constant drilling rate and add this depth-dependent drilling period to the first relaxation period to obtain a start time for ice growth for first closure, t_{s1}. The second reaming of the hole, which was assumed to return the hole to its initial 600 mm diameter, was completed 114 hours after the first. The effective start time for second closure, t_{s2}, is therefore the sum of this 114 hour period and the 9 hour relaxation period after the second reaming during which the water cools (see Fig. 5).

After each relaxation period ends, we require that the heat flux (Eqn (6)) be calculated at the moving ice/water interface, $r = R$. We assume that the heat conducted through the cylindrical surface $r = a$ is approximately the same as the heat transferred through the surface $r = R$ where freezing occurs, i.e. that there are no sources or sinks of heat in $R < r < a$. The purpose of this assumption is to ignore the complex details of heat transfer in the refrozen ice, where we lack detailed knowledge of thermal parameters.

As described above, the ice that grows is porous and the liquid fraction is assumed interconnected. This allows convection to occur, resulting in a significantly greater rate of heat transfer in comparison to conduction in the host ice. The effective thermal conductivity of the new ice will be denoted K_{eff} and it is assumed $K_{eff} \gg K_{ice}$ because of convective heat transfer. After some ice has formed (Fig. 10a), the heat flux must be continuous at $r = a$:

$$-K_{eff}\left[\frac{\partial T}{\partial r}\right]_{r\to a^-} = -K_{ice}\left[\frac{\partial T}{\partial r}\right]_{r\to a^+} \tag{7}$$

Because $K_{eff} \gg K_{ice}$ the temperature gradient inside the boundary at $r = a$ must be much smaller than it is outside (Fig. 10b). The large value of K_{eff} will mean that the refreezing ice is in a pseudo steady state, because it takes longer for the ice to grow than it does to reach an equilibrium temperature distribution. The general solution to the temperature distribution in the annulus is given by Carslaw and Jaeger (1959):

$$T(r) = A + B\ln(r) \qquad R < r < a \tag{8}$$

A and B can be found from the boundary temperatures. Thus the new porous ice is approximately isothermal with the water in the hole.

There is further support from analogous measurements in the sub-ice platelet layer at the base of sea ice. Gough and others (2012) state that temperature measurements in the sub-ice platelet layer are within 0.1°C of the ocean measurements a few metres from the ice, despite the presence of a temperature gradient of the order $10^{\circ}\mathrm{C\,m^{-1}}$ in the solid ice above. Hereafter all the points $r < a$ will be treated as isothermal (equal to T_w). This will become invalid for small values of R/a.

The heat flux into the ice, f_{ice}, can now be approximated for all values of time using Eqn (6). It is equated to the flux of latent heat from growth of an annulus, area A', of porous ice

https://doi.org/10.3189/2013JoG12J117 Published online by Cambridge University Press

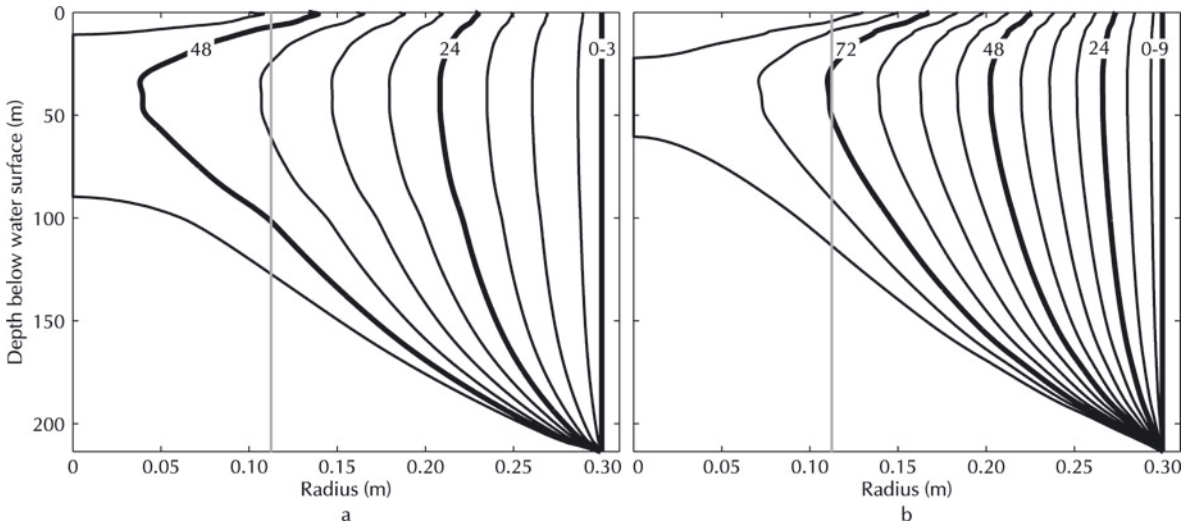

Fig. 11. (a) Evolution of the borehole radius, R, during (a) first closure and (b) second closure for $\phi = 0.5$. Thin curves are separated by 6 hours and thick curves by 24 hours, with time measured relative to the moment the reamer is removed from the hole. Ice growth is delayed by 3 and 9 hours for first and second closure, respectively (see text). The vertical grey lines indicate the radius of the CTD profiler frame.

to find the refreezing rate:

$$f_{\mathrm{ice}} = f_{\mathrm{latent}} = \phi \rho L_{\mathrm{f}} \frac{\mathrm{d}A'}{\mathrm{d}t} \frac{1}{2\pi a} \tag{9}$$

Rewriting $\mathrm{d}A'/\mathrm{d}t$ in terms of the desired quantity, $\mathrm{d}R/\mathrm{d}t$,

$$\frac{\mathrm{d}A'}{\mathrm{d}t} = -2\pi R \frac{\mathrm{d}R}{\mathrm{d}t} \tag{10}$$

leads to

$$-\phi \rho L_{\mathrm{f}} \frac{R}{a} \frac{\mathrm{d}R}{\mathrm{d}t} = f_{\mathrm{ice}}(t) \tag{11}$$

$$\int_a^R -R' \,\mathrm{d}R' = \frac{a}{\phi \rho L_{\mathrm{f}}} \int_{t_{\mathrm{s}}}^t f_{\mathrm{ice}}(t') \,\mathrm{d}t' \tag{12}$$

$$R(t - t_{\mathrm{s}}) = \sqrt{a^2 - \frac{2a}{\phi \rho L_{\mathrm{f}}} \int_{t_{\mathrm{s}}}^t f_{\mathrm{ice}}(t') \,\mathrm{d}t'} \tag{13}$$

where time is measured relative to the moment ice growth starts, with t_{s} denoting either t_{s1} or t_{s2}, depending on the scenario considered.

The results of this derivation are shown in Figure 11. An interesting aspect of the result is that the part of the hole with the highest refreezing rate is not the top of the hole where the ice is coldest. Rather, the air trapped in the ice near the surface reduces the rate of heat transfer, such that the hole refreezes more slowly in the upper 30 m of the water-filled hole.

DISCUSSION

We are now in a position to compare the two calculations of refreezing formulated in the previous sections. Each calculation requires different assumptions and has its own merits and the best prediction of refreezing results from a combination of the methods. A comparison of the predicted refreezing rates is shown in Figure 12 for both first and second closure.

Prediction of the refreezing rates using the salinity variation calculation (SVC) requires a value for the hole's radius at the time the CTD casts began. This was not measured directly. Instead we estimate the ice growth during this time by extrapolation of the average growth predicted during the CTD casts. This yields a 40 mm decrease in diameter before the casts began.

It is likely that the heat-flux model (HFM) overestimated the rate of ice growth during first closure. No direct measurements of the refreezing rates were made on site, but the hole diameter was known to be larger than the CTD profiler's 225 mm diameter frame when CTD measurements ended 42 hours after reaming. Figure 11a shows that the hole's radius is predicted to fall below this value at approximately this time at depths around 50 m. During second closure the host ice had warmed significantly and we predict a period of 72 hours before the hole diameter falls below 225 mm. Further, there is a significant discrepancy between the refreezing rates predicted by the SVC and HFM during first closure. On average, the results differ by a factor of 3.7. For second closure, the SVC and HFM agree, within error, in the top seven of ten depth bins.

It is expected that the refreezing rates show some dependence with depth. More specifically, the water should freeze most quickly near the top, where the host ice is coldest. Makinson (1993) presents direct calliper measurements of refreezing rates in a borehole in the Ronne Ice Shelf that suggest this predicted behaviour. The SVC shows lesser depth dependence. Above 70 m the trend is similar to that of the HFM, while below 70 m the rate is approximately constant with depth.

In the range 20–80 m the water was either neutrally or stably stratified (Fig. 2c and g). Here the SVC predicts the same refreezing rate for first and second closure, within error. Below 80 m the SVC predicts the unlikely result that the hole refroze more slowly during first closure. This region largely corresponds to that in which a negative buoyancy frequency was observed, an indication that turbulent vertical diffusion of salt and advection of salt water through the base of the hole cannot both be ignored. Hence, we have more confidence in the predictions for second closure than we do for those in the first closure, when significant instability was observed (Fig. 2c).

A major focus of this study is to simulate the refreezing of the ANDRILL borehole, but it is desirable to apply the models elsewhere. The calculation of the refreezing rate from the SVC predicts only an expected rate for a similarly

https://doi.org/10.3189/2013JoG12J117 Published online by Cambridge University Press

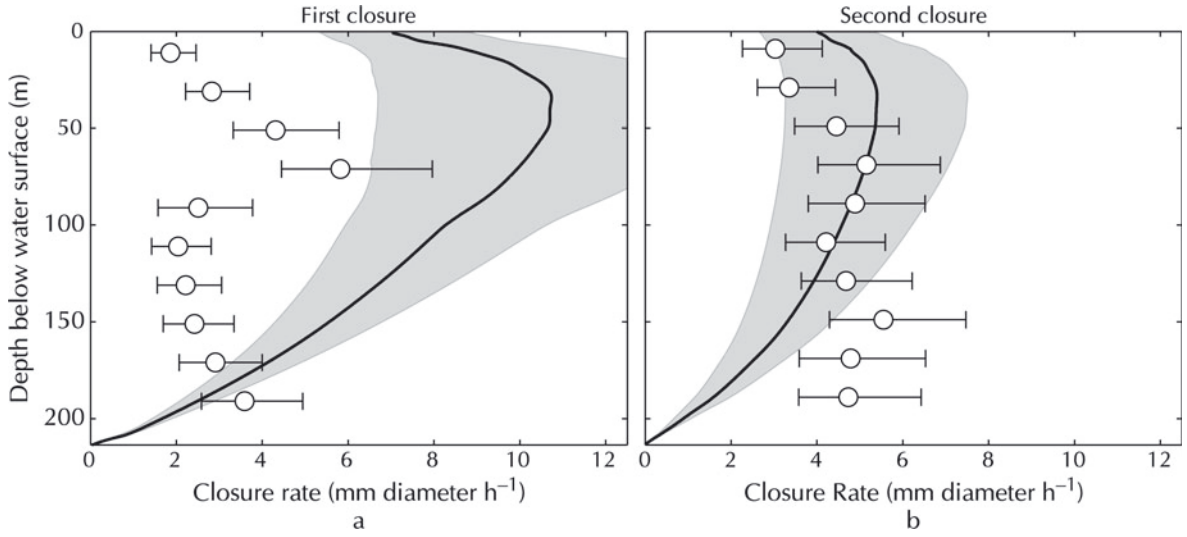

Fig. 12. Comparison of the refreezing rates calculated from salinity measurements (markers, 20 m depth averages) and the heat-flux model (curves). Refreezing rates, averaged over the period CTD casts were taken, are the gradient of a least-squares, linear fit to the radius over time. Uncertainties in the SVC (salinity variation calculation) results are due to both the standard error of the refreezing rate (Fig. 8) and the uncertainties in initial radius and the value of ϕ. Uncertainty in the HFM (heat-flux model) results, shown by the grey swath, is due to uncertainty in ϕ and the initial radius.

sized borehole in a similar location. Conversely, application of the HFM to an alternative site is possible.

Accurate application of the HFM at a different location would require ice-shelf temperature and density profiles, at or near the alternative site. Other thermal parameters can be derived from these, as described above. However, temperature profiles through Antarctic ice shelves have been measured at a very limited number of locations (e.g. Clough and Hansen, 1979; Rist and others, 2002). A solution is to assume all Antarctic ice shelves have similarly shaped temperature and density profiles. Then it is possible to adopt the profiles of Figure 10 by vertically scaling them to fit the thickness of the ice shelf in question. Humbert and others (2005) used a vertical scaling of a single parabolic fit to model the temperature profile for the entire Ross Ice Shelf. Further, Makinson (1993) presents the temperature profile through the Ronne Ice Shelf which, despite being almost twice as thick and having a different surface temperature, has a very similarly shaped profile to that of Bender and Gow (1961). If it is assumed that the profiles of all parameters show this scaling behaviour then it would be possible to implement this model elsewhere, knowing only the temperature in the top section of the ice shelf, for which there are a number of datasets (e.g. MacAyeal and others, 2008).

Some parameters may even be treated as constant. For example, T_w cannot be known without a CTD cast being taken, but its range is only a few degrees and could be taken as -1°C everywhere without much loss of accuracy. We repeated our calculations with all parameters, except the host ice temperature, fixed with respect to depth. The refreezing rates differed by a maximum of 11% and 6% for first and second closure, respectively. The predictive ability of the HFM is best for a borehole that has been kept open for a number of days. This allows the heat flux to come to a nearly steady value and reduces the importance of the estimate of the initial conditions.

Our study is most applicable to large holes (>0.5 m) in which the time to reach closure is of the order of 5–10 times longer than the drilling period. We have ignored factors, such as refreezing during the drilling process and heat loss through the length of the hose, which become significant when drilling deeper, narrower holes (e.g. Napoléoni and Clarke, 1978; Humphrey and Echelmeyer, 1990).

CONCLUSION

Two sets of ten CTD casts were taken, each over 28 hours, and ~5 days apart, through a 600 mm diameter borehole in a 252 m thick region of the Ross Ice Shelf. The water column was effectively decoupled from the ocean below due to a strong density gradient near the base of the hole, and measurements indicated that a large portion above this was persistently supercooled. The geometry of the hole implies that turbulent mixing was presumed to occur inside this closed system, on scales approximately equal to or less than the diameter of the hole. In spite of this mixing, it was shown that the hole supported a large density inversion for more than 24 hours, which we attribute to the large aspect ratio of the hole.

The rate of refreezing of the borehole, which was surrounded by ice with a minimum temperature of -22°C, was calculated by two independent methods. The first was based on salt conservation in the hole and predicted likely refreezing rates in the range 3–5 mm diameter h^{-1} (Fig. 12b). The second equated the latent heat released by freezing to the divergence of the conductive heat flux at the cylindrical surface of the hole.

Hole closure was modelled on two occasions, the first immediately after reaming of the hole, the second after the hole was re-reamed 5 days later. The salinity calculation yielded closure rates that are within error on both occasions in regions where the fluid in the hole was neutrally or stably stratified. Further, the HFM on second closure agreed with these rates in seven of the ten depth bins. However, the HFM predicted rates for first closure that were approximately double that for the second closure.

The amount of time a borehole takes to refreeze is dependent on the structure of the refrozen ice. In this study

https://doi.org/10.3189/2013JoG12J117 Published online by Cambridge University Press

the treatment of this structure was reduced to an estimate of the solid fraction, ϕ, on the assumption that ice freezes with a porous structure and that a fixed fraction of solid ice grows in any volume of supercooled water. The instantaneous refreezing rates predicted are directly proportional to the ice solid fraction chosen. Knowledge of the thermal properties of the refrozen ice would reduce the uncertainty associated with the choice of the value of ϕ, and allow a better estimate of the heat flux through the freezing interface.

Our study indicates that borehole refreezing rates derived from down-hole measurements broadly confirm the reliability of applying a simple thermodynamic model to scenarios in which the dependence on the initial conditions is small. Our method, which contains many estimates, would benefit from improved knowledge of a number of parameters. The relaxation period after reaming could easily be measured using temperature probes within the borehole, or by taking multiple CTD casts in quick succession immediately after drilling. In addition, the nature of the refrozen borehole wall, as well as the processes of frazil ice production and deposition, could be further analysed with down-hole video.

ACKNOWLEDGEMENTS

We are grateful to the ANDRILL team at Coulman High for making and maintaining the boreholes and assistance with data collection. We particularly thank Tamsin Falconer for providing the hot-water drilling records, Craig Stewart for measuring heights in the ice shelf, Craig Stevens and the three anonymous reviewers for comments on this paper, and Angelika Humbert for comments regarding Ross Ice Shelf temperatures. We are grateful for logistical support from Antarctica New Zealand and the United States Antarctic Program. The data collection was funded by the New Zealand Ministry of Business, Innovation, and Employment (contract No. C05X1001), and NIWA core funding under the National Climate Centre Research Programme 2 (2011–12 and 2012–13), and support was provided by a University of Otago Research Grant to write this paper.

REFERENCES

Arakeri JH, Avila FE, Dada JM and Tovar RO (2000) Convection in a long vertical tube due to unstable stratification – a new type of turbulent flow? *Current Sci.*, **79**(6), 859–866

Bender JA and Gow AJ (1961) Deep drilling in Antarctica. *IASH Publ.* 55 (General Assembly of Helsinki 1960 – *Antarctic Glaciology*), 132–141

Carslaw HS and Jaeger JC (1986) *Conduction of heat in solids*, 2nd edn. Oxford University Press, Oxford

Cholemari MR and Arakeri JH (2009) Axially homogeneous, zero mean flow buoyancy-driven turbulence in a vertical pipe. *J. Fluid Mech.*, **621**, 69–102 (doi: 10.1017/S0022112008004254)

Clough JW and Hansen BL (1979) The Ross Ice Shelf project. *Science*, **203**(4379), 433–434 (doi: 10.1126/science.203.4379.433)

Fofonoff NP and Millard RC, Jr (1983) Algorithms for computation of fundamental properties of seawater. *UNESCO Tech. Pap. Mar. Sci.* 44

Foster TD (1983) The temperature and salinity fine structure of the ocean under the Ross Ice Shelf. *J. Geophys. Res.*, **88**(C4), 2556–2564 (doi: 10.1029/JC088iC04p02556)

Gough AJ, Mahoney AR, Langhorne PJ, Williams MJM, Robinson NJ and Haskell TG (2012) Signatures of supercooling: McMurdo Sound platelet ice. *J. Glaciol.*, **58**(207), 38–50 (doi: 10.3189/2012JoG10J218)

Harrison WD (1972) Temperature of a temperate glacier. *J. Glaciol.*, **11**(61), 15–29

Haynes WM ed. (2010) *CRC handbook of chemistry and physics*, 91st edn. CRC Press, Boca Raton, FL

Huang JS and Barduhn AJ (1985) The effect of natural convection on ice crystal growth rates in salt solutions. *AIChE J.*, **31**(5), 747–752 (doi: 10.1002/aic.690310507)

Humbert A, Greve R and Hutter K (2005) Parameter sensitivity studies for the ice flow of the Ross Ice Shelf, Antarctica. *J. Geophys. Res.*, **110**(F4), F04022 (doi: 10.1029/2004JF000170)

Humphrey N and Echelmeyer K (1990) Hot-water drilling and borehole closure in cold ice. *J. Glaciol.*, **36**(124), 287–298

Jacobs SS, Gordon AL and Ardai JL, Jr (1979) Circulation and melting beneath the Ross Ice Shelf. *Science*, **203**(4379), 439–443 (doi: 10.1126/science.203.4379.439)

Kreith F and Romie FE (1955) A study of the thermal diffusion equation with boundary conditions corresponding to solidification or melting of materials initially at the fusion temperature. *Proc. Phys. Soc. B*, **68**(5), 277–291 (doi: 10.1088/0370-1301/68/5/302)

Leonard GH, Purdie CR, Langhorne PJ, Haskell TG, Williams MJM and Frew RD (2006) Observations of platelet ice growth and oceanographic conditions during the winter of 2003 in McMurdo Sound, Antarctica. *J. Geophys. Res.*, **111**(C4), C04012 (doi: 10.1029/2005JC002952)

MacAyeal D, Sergienko O and Muto A (2008) *Ross Ice Shelf firn temperature, Antarctica,* National Snow and Ice Data Center, Digital media: http://nsidc.org/data/nsidc-0345.html

Mahoney AR and 6 others (2011) The seasonal appearance of ice shelf water in coastal Antarctica and its effect on sea ice growth. *J. Geophys. Res.*, **116**(C11), C11032 (doi: 10.1029/2011JC007060)

Makinson K (1993) The BAS hot water drill: development and current design. *Cold Reg. Sci. Technol.*, **22**(1), 121–132 (doi: 10.1016/0165-232X(93)90051-9)

Napoléoni JGP and Clarke GKC (1978) Hot water drilling in a cold glacier. *Can. J. Earth Sci.*, **15**(2), 316–321

Petrich C, Langhorne PJ and Haskell TG (2007) Formation and structure of refrozen cracks in land-fast first-year sea ice. *J. Geophys. Res.*, **112**(C4), C04006 (doi: 10.1029/2006JC003466)

Poots G (1962) On the application of integral-methods to the solution of problems involving the solidification of liquids initially at fusion temperature. *Int. J. Heat Mass Transfer*, **5**(6), 525–531 (doi: 10.1016/0017-9310(62)90163-1)

Rack FR and 30 others (2012) What lies beneath? Interdisciplinary outcomes of the ANDRILL Coulman High Project site surveys on the Ross Ice Shelf. *Oceanography*, **25**(3), 84–89 (doi: 10.5670/oceanog.2012.79)

Rist MA, Sammonds PR, Oerter H and Doake CSM (2002) Fracture of Antarctic shelf ice. *J. Geophys. Res.*, **107**(B1) (doi: 10.1029/2000JB000058)

Schwerdtfeger P (1963) The thermal properties of sea ice. *J. Glaciol.*, **4**(36), 789–807

Weeks WF (2010) *On sea ice*. University of Alaska Press, Fairbanks, AK

APPENDIX A. BOREHOLE RAYLEIGH NUMBER

The gradient Rayleigh number is defined as

$$\mathrm{Ra_g} = \frac{g}{\rho}\frac{\mathrm{d}\rho}{\mathrm{d}z}\frac{d^4}{\nu\alpha} \qquad \text{(A1)}$$

where d is the diameter, g is acceleration due to gravity, ν is kinematic diffusivity of water ($\nu = 1.8 \times 10^{-6}\,\mathrm{m^2\,s^{-1}}$ for water with $T = 0°\mathrm{C}$ and $S = 5$) and α is the diffusivity

https://doi.org/10.3189/2013JoG12J117 Published online by Cambridge University Press

of species creating the density difference, i.e. salt ($\alpha = 8 \times 10^{-10}\,\mathrm{m^2\,s^{-1}}$).

For a cylinder containing a fluid with an unstable density gradient, Arakeri and others (2000) found that flow within a cylinder became turbulent when the gradient Rayleigh number, $\mathrm{Ra_g}$, exceeded 10^7. Below 10^7, depending on the Rayleigh number, the flow was one of the following: laminar, consisting of one up- and one down-flowing stream; helical; or unsteady, but laminar. Observed unstable gradients inside the borehole were typically $0.01\,\mathrm{kg\,m^{-4}}$, yielding $\mathrm{Ra_g} = 9 \times 10^9$, which is well within the turbulent regime.

APPENDIX B. ITERATION PROCEDURE

A predictor–corrector scheme is used to implement the salinity-based refreezing rate iteration, Eqn (2). This states $R_{i+1} = h(S_i, S_{i+1}, R_i)$, i.e. the next radius value is dependent on the current radius and the current and following salinity values and h denotes their relationship. The procedure finds R_{i+1} by first calculating the trial values $\widetilde{R}_{i+1}$ and $\widetilde{R}_{i+2}$ directly from Eqn (2). R_{i+1} is then predicted from the average growth rate between t_i and t_{i+2}.

Mathematically this is stated as

$$\widetilde{R}_{i+1} = h(S_i, S_{i+1}, R_i) \tag{B1}$$

$$\widetilde{R}_{i+2} = h(S_{i+1}, S_{i+2}, \widetilde{R}_{i+1}) \tag{B2}$$

Letting $\Delta t_i = t_{i+1} - t_i$

$$R_{i+1} = \frac{1}{2}\left(\frac{\widetilde{R}_{i+1} - R_i}{\Delta t_i} + \frac{\widetilde{R}_{i+2} - \widetilde{R}_{i+1}}{\Delta t_{i+1}}\right)\Delta t_i \tag{B3}$$

The final value for the radius is found directly from Eqn (2) using only values at t_{i+1} as there is no t_{i+2}.

MS received 2 July 2012 and accepted in revised form 4 June 2013

https://doi.org/10.3189/2013JoG12J117 Published online by Cambridge University Press